electronics

MDPI

Article

Development of a Grinding Tool with Contact-Force Control Capability

Yu-Heng Lin, Ming-Wei Liu and Pei-Chun Lin *

Department of Mechanical Engineering, National Taiwan University (NTU), No.1 Roosevelt Rd. Sec. 4, Taipei 106, Taiwan; r08522824@ntu.edu.tw (Y.-H.L.); r07522856@ntu.edu.tw (M.-W.L.)
* Correspondence: peichunlin@ntu.edu.tw

Abstract: The grinding normal force is one of the main factors that affect grinding quality. We report on the development of a compact grinding tool which not only can rotate the grind wheel but also can actively control the wheel in the fore/aft direction to modulate the contact force. The two motion degrees of freedom are coupled in the sense of mechanism yet their motions are independent. The designed grinding tool was modeled and its parameters were systemically identified. A repetitive controller was designed to suppress periodic force variation, which was mainly caused by the rotational motion of the grinding wheel, and the results were compared with other control methods. The selection of the grinding parameters was conducted using the Taguchi method. Finally, the grinding tool and the repetitive controller were experimentally evaluated, and the experimental results confirm that the proposed control strategy can reduce the force disturbance and improve the surface quality of the flat and curvy workpieces.

Keywords: grinding tool; force control; modeling; surface roughness; peak filter; repetitive control; Taguchi method

Citation: Lin, Y.-H.; Liu, M.-W.; Lin, P.-C. Development of a Grinding Tool with Contact-Force Control Capability. *Electronics* **2022**, *11*, 685. https://doi.org/10.3390/electronics11050685

Academic Editor: Davide Astolfi

Received: 31 December 2021
Accepted: 21 February 2022
Published: 23 February 2022

1. Introduction

The grinding process is regarded as an essential part of machining in the metal manufacturing industry. It is used to remove surface defects and material and to reduce the surface roughness for a better quality of the next process, which may be polishing or electroplating. For years, the grinding process has been executed manually, but this is time-consuming and generates harsh noise and a dusty environment that is harmful to laborers. Furthermore, it takes a high amount of resources and time for training and recruiting sufficiently high-skilled workers.

For the intention of solving the manual limitations mentioned above, some industries and researchers have dedicated efforts to seeking and developing alternative solutions in the industrial automation domain. Extensive work has focused on robot path planning for its repeatability, precision, and durability. Classical robot path planning methods may achieve the requirements of some operations, such as welding and laser cutting, for which contact and the precision of the position are not necessary. However, for some contact operations, including polishing, grinding, and assembling, it is necessary to maintain a stable contact force between the manipulators and the workpiece other than path planning [1]. First, the robot trajectory may have minor fluctuations because of the low stiffness of the series structure and the large inertia load. Second, the contact point gradually deviates from the original trajectory due to the wear of the grinding tool and deformation of the workpiece under intense interaction. Moreover, deviation in the material-removal rate emerges [2–6], caused by a deviated contact force; as a result, an uneven surface is formed.

Force control and feedback based on various kinds of sensors is a straightforward method to solve the problems described above, on which various works have reported. For example, Wang et al. proposed a normal force-estimation model for a belt-grinding

system [7]. Zhang et al. reported a wheel wear monitoring system using an interval type-2 fuzzy basis function network [8]. Xu et al. reported a hybrid active/passive force-control strategy [9] and hybrid force/position anti-disturbance control strategy [10] for grinding marks suppression in robotic belt grinding of turbine blade. Dai et al. proposed a constant force control strategy combined by extended state observer and backstepping control [11]. Kuma and Rani developed a neural network-based hybrid force/position control [12].

In the manipulator-based control applications, we can identify two main control strategies—through the arm and around the arm. The former directly controls each axis of the manipulator using its torque and angle feedback. Hybrid control combines the advantages of position control and force control. A parallel control structure was proposed in [13]; this revises the planned trajectory in real time with force and position control. In [14], an adaptive control strategy was proposed, involving a combination of a closed-loop position control and an open-loop force control to compensate for contact forces. Another commonly used strategy is impedance control, which is a method based on positional adjustment. Lee and Buss [15] proposed an impedance-control strategy in which target stiffness was varied online to regulate the desired contact force without any knowledge of the environment. Jung et al. [16] presented an impedance-control scheme with the ability to track a specified desired force and to compensate for uncertainties in environment, location and stiffness, as well as in the robot dynamic model. The control strategy was different before and after contact with the environment. In addition to the two mainstream control schemes mentioned above, sliding-mode control was also utilized. In [17], Zhang et al. presented an adaptive sliding mode via an iterative constant-force control method that gradually reduced the grinding force fluctuation during the iterations. Lu et al. [18] presented a method that combined sliding-mode and impedance control. By using the PI controller, the oscillation during the convergence of the sliding mode can be reduced. Furthermore, the impedance parameters were chosen by analyzing the grinding-force spectrum.

Although the concept of through the arm is more intuitive and low-cost than around the arm, it is hard to implement the algorithm and difficult to achieve a significant improvement because of the weak stiffness and coupling effect of the multi-axis structure. In addition, it is hard to achieve in a commercial manipulator owing to the limited communication bandwidth. In contrast, the around-the-arm approach designs an additional end effector that is controlled independently of the manipulator. Kuo et al. [19] designed a force regulation mechanism to be installed on grinding tools, which can passively produce an adjustable normal contact force with a special spring. Liao et al. [20] developed a new approach for the modeling and control of an automated polishing process that utilized a dual-purpose compliant toolhead with three pneumatic actuators to provide tool compliance. In [21], Mohammad et al. presented a novel design of a force-controlled end effector for automatic polishing. The moving inertia was reduced by the design and arrangement of the mechanism. In [22], an electromagnetism-based compliant polishing device was designed, and a force control strategy based on PD control and BP neural networks was also proposed; however, this design proves to be too heavy for a lightweight manipulator. Ma et al. [23] developed a parallel mechanism that ensures the six degrees of freedom of the grinding tool. By using PD controllers, the grinding force can be compensated for in a specific direction. Finally, Zhang et al. [24] reported that normal force is the main factor that affects surface roughness.

Motivated by the research described above and following our initial presentation in [25], in this work, a contact-force-controlled grinding tool is developed. The contribution of this research is summarized as follows:

- A compact electric grinding tool is designed, with highly dynamic and controlled fore/aft spindle motion while the grinding wheel is spinning. No pneumatic system is required.
- A model-based system identification is utilized for controller design.

- The possible force disturbance is analyzed so the corresponding force control strategy can be deployed.
- The surface roughness of the grinded workpiece is improved using the proposed grinding tool with repetitive controller. The controller greatly suppresses the vibration caused by the rotation of the grinding wheel.

Compared with the existing design, the proposed design has a smaller form factor while maintaining its functionality. By doing so, the agility of the grinding tool is greatly improved with little sacrifice in terms of grinding power. In addition, a repetitive controller was also implemented to suppress the internal vibration caused by the unbalanced low-cost grinding wheel, thereby achieving better performance compared with other systems.

The remainder of the paper is organized as follows: In Section 2, the design is introduced, and the model of the mechanism is built and subsequently utilized in system identification. In Section 3, we briefly analyze the controlling target that needs to be suppressed and design a PID controller with a peak filter for force tracking and disturbance rejection. Simulation is then built for the verification of the controller design. In Section 4, the grinding experiment results are reported to validate the performance of the proposed system. Section 5 concludes the work.

2. Mechanical Design, Modeling, and System Identification of the Grinding Tool

2.1. Mechanical Design

To accomplish the desired grinding performance, the design criteria of the grinding tool are proposed as follows:

- While the grinding wheel spins, the grinding tool is capable of a highly dynamic and actively controlled fore/aft motion to adjust the normal contact force in real time.
- To implement force control, a force sensor should be included; it should be mounted as close to the contact point as possible to reduce the possible disturbance in the tool, such as backlash and elastic deformation.
- The overall length of the grinding tool should be as short as possible to ease the manipulation when grinding. This characteristic is particularly useful when the tool is mounted on the manipulator, which maintains operation maneuverability.
- The mass of the grinding module should be small. In addition, a simple yet rigid structure is desired.

Based on these criteria, a hollow voice coil motor (HVCM) was utilized for fore/aft motion of the grinding wheel, where the motor could perform large and rapid force output compared with other linear actuators. The hollow axis of the motor allows the rotating shaft of the grinding axis to pass through. A brushless DC (BLDC) motor was chosen to drive the grinding wheel. Compared with other types of motors, BLDC motors generally have high power density. The large diameter of the motor also provides higher direct-drive torque. To reduce the payload of the HVCM, the BLDC should be mounted at the fixed end, and only the grinding wheel should be moved by the HVCM for fore/aft motion. The key of the mechanical design is ensuring simultaneous but independent operation of two actuators, which implies that a transmission mechanism that can carry a high load of torque while performing linear moving is necessary. As a result, a ball spline is used to serve as the transmission mechanism. The spline shaft of the ball spline contains grooves that provide a large moment load-carrying capacity. The balls in the spline nut reduce the influence of friction and achieve a smooth motion on the grooves. To mount the force sensor close to the grinding wheel, as well as to provide space for the grinding shaft, a force sensor with a through-hole was chosen.

Figure 1 shows a sectional view of the entire grinding tool. The tool frame has two parts, and the fixed tool frame on the left side was designed to mount to the work station or the end of the manipulator. The moving tool frame was designed to mount the grinding wheel (No. 11), which can simultaneously rotate and move in the fore/aft direction for position and force adjustment. Three linear slides (no.3) were mounted between these two tool frames, allowing the moving tool frame to have only one degree-of-freedom (DOF)

fore/aft motion in relation to the fixed tool frame. This DOF was driven and controlled by the HVCM (no.5). One side (i.e., the left side) of the BLDC (no.2) was mounted to the tool frame, and here, the rotating part of the motor is connected to and drives the spline shaft (no.1) of the ball spline (no.7). The rotational motion of the spline shaft driven by the BLDC rotates the ball spine, which then transmits the rotational motion to the grinding shafts A (no.9) and B (no.10), driving the grinding wheel. The ball spline and shafts A and B are fixed on the moving tool frame with a thrust roller bearing (no.8). Thus, while the moving tool frame can only move in the fore/aft direction, the shaft can still rotate to perform grinding motion.

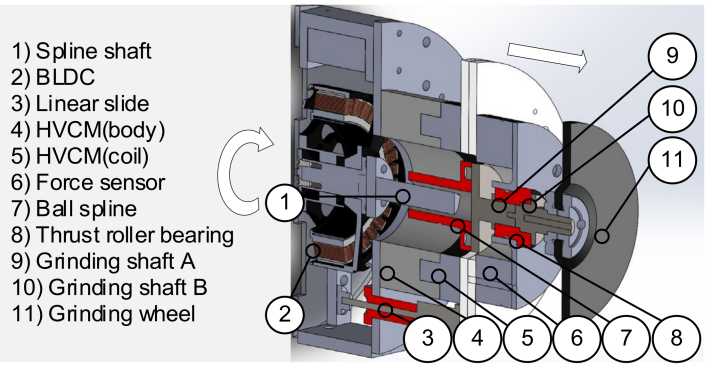

Figure 1. Section view of the CAD drawing of the designed grinding tool.

During the grinding process, the grinding wheel should be controlled to eliminate oscillation, filter out noises, and reduce impact while interacting with the workpiece. When the grinding wheel contacts the workpiece, the contact force is transmitted to the thrust-roller bearing mounted on the force sensor. Therefore, the force sensor can measure the contact force without much energy loss. With the in situ force data, the HVCM can modulate the grinding force according to the desired force profile. The configuration of the grinding tool was designed to have the minimum mass of the moving part, so the grinding wheel can be actuated in a highly dynamic manner.

Compared with traditional grinding tools, the proposed design has the following advantages:

- Using the voice coil motor as the actuator can provide a controllable and high-frequency response compared with other methods. Dynamic elimination and stability control can result in better performance.
- The actuator for grinding (i.e., the BLDC) remains stationary on the fixed frame, and only its motion is transmitted to the grinding wheel. Compared with the design that mounts the entire rotary system on the moving frame, the proposed design significantly reduces the payload to the linear actuator (i.e., HVCM) and the resulting vibration and noise.
- The force sensor is mounted very close to the grinding wheel for accurate contact-force measurement.
- The overall length of the grinding tool is only about 20 cm, and its weight is only 4 kg, so it can be mounted and operated on the end of the mainstream manipulator.

2.2. System Modeling

To make the controller design more intuitive, a physical model of the grinding tool was constructed, and its dynamic behavior was then analyzed. The model includes both the electrical model of the motor and the mechanical model of the tool, as shown in Figure 2.

The simplified free-body-diagram of the grinding tool is illustrated in Figure 3. The equation of motion (EOM) is:

$$M\ddot{x}(t) = F_v(t) - c\dot{x}(t) - (F_t + Mg). \quad (1)$$

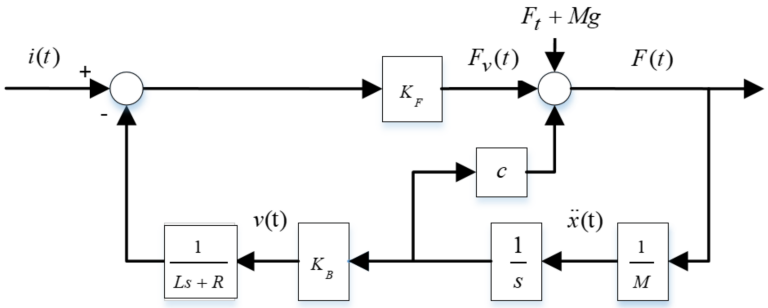

Figure 2. Block diagram of the grinding tool.

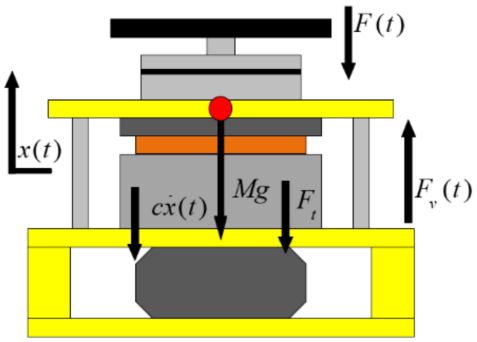

Figure 3. Free body diagram of the grinding tool.

The friction force F_t can be neglected owing to use of the linear bearings, and the gravity effect can be compensated for by the constant force shifting. Thus, the EOM can be simplified as:

$$M\ddot{x}(t) = F_v(t) - c\dot{x}(t). \tag{2}$$

Considering the back electromotive force(EMF) [26] generated when the coil is rapidly oscillating and the force decay caused by displacing of the coil, the dynamic equation is as follows:

$$F_v(t) = K_F[i_a(t) - i_b(t)] - K_l x(t), \tag{3}$$

$$i_b(t) = \frac{1}{L}e^{-\frac{R}{L}t}v_b(t) = \frac{1}{L}e^{-\frac{R}{L}t}K_B\dot{x}(t). \tag{4}$$

where K_F, K_I, $i_b(t)R$, and L are the proportional constant between the current and the force, the effective coefficient of the force decade effect, the current caused by the back EMF, the resistance of the HVCM, and the inductance of the HVCM, respectively. The force decay effect can be neglected because the working stroke is limited to a short distance. Hence, substituting Equations (3) and (4) into Equation (2) yields the following:

$$M\ddot{x}(t) = K_F[i_a(t) - \frac{1}{L}e^{-\frac{R}{L}t}K_B\dot{x}(t)] - c\dot{x}(t). \tag{5}$$

By performing Laplace transform, the open loop transfer function of the model from motor current to displacement of the moving tool frame as calculated as follows:

$$\frac{X(s)}{I(s)} = \frac{K_F(Ls+R)}{MLs^3 + (CL+MR)s^2 + (CR+K_FK_B)s}. \tag{6}$$

To better analyze the force dynamic, replacing the output in Equation (6) from displacement $X(s)$ to contact force $F(s)$, we obtain a second-order transfer function:

$$\frac{F(s)}{I(s)} = \frac{K_F Ms(Ls + R)}{MLs^2 + (CL + MR)s + CR + K_F K_B}. \tag{7}$$

Following this model, system-identification can then be performed to obtain parameters of the model, which is helpful for the design and simulation of the controller.

2.3. System Identification

Gray-box transfer function estimation was utilized because the order of the numerator and denominator is bounded. An autoregressive with exogenous (ARX) model was chosen:

$$A(z)y[k] = B(z)u[k] + e[k], \tag{8}$$

where $y[k]$ is the output, $u[k]$ is the input, and $e[k]$ is white noise independent of the input. With knowledge of the physical model, the discrete-time iterative equation is written as follows:

$$y[k] = a_1 y[k-1] + a_2 y[k-2] + b_1 u[k-1] + b_2 u[k-2] + e[k]. \tag{9}$$

The problem addressed in this section is the estimation of the parameters a_n and $b_{n,\ n=1,\ 2}$ based on incomplete observations of $y[k]$ and $u[k]$, in this case, the force generated by HVCM and input commands of the servo amplifier. Chirp sine, as shown in Figure 4a, was used for the input command to better capture the response of the system under different frequencies.

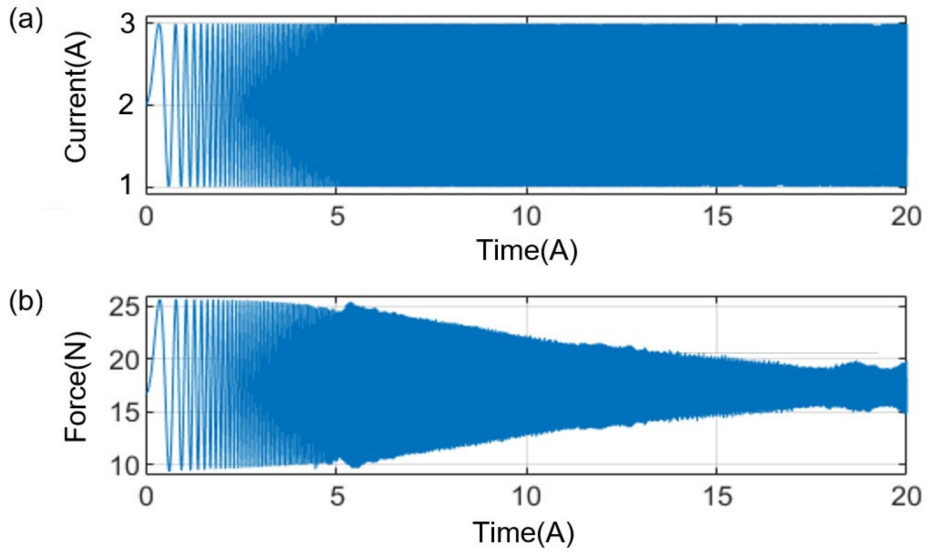

Figure 4. System identification of the grinding tool: (**a**) Chirp sine as the input and (**b**) force as the output.

Using the nonlinear least square method, a fitted linear discrete-time model was generated with an accuracy of 86.51%, as shown in Figure 5. The corresponding transfer function is

$$G(z) = \frac{-0.0001967z^{-1} + 0.0005895z^{-2}}{1 - 1.621z^{-1} + 0.6669z^{-2}}. \tag{10}$$

The controller design and subsequent simulation can be carried out based on the mathematical model shown in Equation (10).

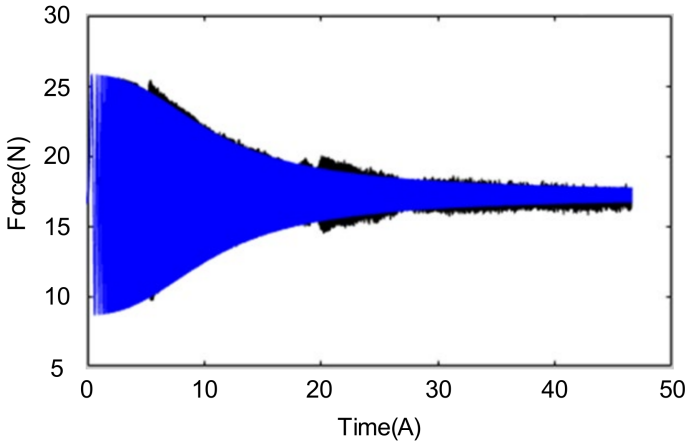

Figure 5. Comparison of the original force data (black) and fitted model (blue).

3. Controller Design and Simulation

During the grinding process, surface undulation of the workpiece and force disturbance may deteriorate the grinding quality. Li, H. [4] summarized the relationship between grinding force and process quality. Some criteria are proposed and summarized as follows. First, a stable-grinding force ensures an even cutting depth on the surface of the workpiece. The position error of the manipulator can also be compensated for. Second, the interaction between the workpiece and the grinding wheel generates vibration, which can be seen as sensor noise to some degree. Judging from the above, the designed controller should be capable not only of tracking the desired force quickly and steadily but also of rejecting the periodic force disturbance. Hence, to eliminate the disturbance, an analysis of disturbance is necessary for a precise rejecting target.

3.1. Force Disturbance Analysis

Because of the abrasive grains of the grinding wheel and the eccentricity caused by installation, the force disturbance is periodic when the grinding wheel executes high-speed rotation. As shown in Figure 6, power spectrums of grinding force under different grinding rotating speeds were measured. It is clear in the figure that the rotating speed and the dominant peaks of the power spectrum are closely related. For example, the frequencies of the dominant peak in Figure 6, which are 52 Hz, 104 Hz, 156 Hz, 208 Hz, and 260 Hz, provide evidence in favor of the above assumption because they are all close to integer multiples of the rotating speed of the grinding wheel, that is, 3000 rpm (50 Hz). To sum up, once the fundamental frequency is suppressed, the following resonance frequencies should also be suppressed, thereby reducing the force disturbance.

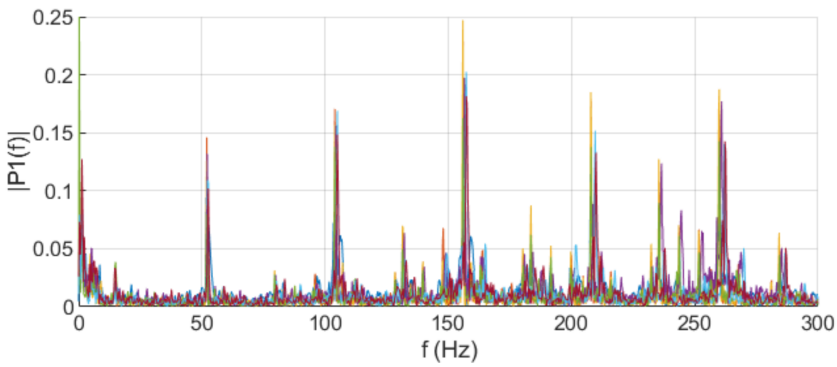

Figure 6. Single-sided amplitude spectrum of the force data when the grinding wheel spins at 3000 rpm (50 Hz).

3.2. Baseline Controller Design

The desired contact force to be generated by HVCM is given as f_d, and the real contact force f is measured by the force sensor. Then, the force tracking error e_f is defined as follows:

$$e_f = f_d - f. \tag{11}$$

For convenience of implementation, the controller was PID-based and directly designed in the discrete-time domain:

$$u(z) = [K_p + K_I(\frac{Ts}{1-z^{-1}}) + K_D(\frac{1-z^{-1}}{Ts})]e_f(z), \tag{12}$$

where K_P, K_I, K_D, and Ts are the proportional gains, integral gains, derivative gains, and sampling time of the system, respectively. To compensate for the gravity effect, a constant offset term u_g was added into the controller, which could be rewritten as

$$u(z) = u_g + [K_p + K_I(\frac{Ts}{1-z^{-1}}) + K_D(\frac{1-z^{-1}}{Ts})]e_f(z). \tag{13}$$

Note that the force provided by the linear actuator has two functions. One is to generate an adequate contact force between the grinding wheel and the work piece, and this is achieved using PID controller. The other is to compensate for the gravity force of the grinding wheel and the associated moving parts of the grinding tool, including parts of numbers 5–11 shown in Figure 1. The offset term u_g compensates for the gravity force. By appropriately selecting the parameters of the controller, the tracking error e_f converges to zero and force-tracking is achieved.

3.3. Peak Filter Design

As described in the first paragraph of Section 3.1, the controller should be designed for suppressing the frequency of the rotating speed, which could be measured empirically using the encoder installed on the BLDC. With a given rotating speed, the frequency was known a priori and could be suppressed. A peak filter [27] is an intuitive choice for manipulating specific frequencies. The equation of the peak filter in the continuous-time domain is

$$Pf(s) = \frac{s^2 + 2kas + \omega^2}{s^2 + 2as + \omega^2}, \tag{14}$$

where ω is the filtered frequency, k adjusts the amplification of the filter ($k > 1$), and a adjusts the width of the filter. The peak filter was transformed into the discrete-time domain for convenience of implementation. The following Tustin transformation [28] was utilized to obtain less distortion during the transformation between the continuous and discrete-time domains:

$$s = \frac{2}{Ts}\frac{1-z^{-1}}{1+z^{-1}}, \tag{15}$$

where Ts is the sampling time. Substituting Equation (15) into Equation (14), the filter can be rewritten as

$$Pf(z) = \frac{(4 + 4kaT_s + {T_s}^2\omega^2) + (2{T_s}^2\omega^2 - 8)z^{-1} + (4 - 4kaT_s + {T_s}^2\omega^2)z^{-2}}{(4 + 4aT_s + {T_s}^2\omega^2) + (2{T_s}^2\omega^2 - 8)z^{-1} + (4 - 4aT_s + {T_s}^2\omega^2)z^{-2}}. \tag{16}$$

A potential problem is that a slight frequency mismatch may occur during the transformation. The peak frequency in the discrete-time domain is not the same as that in the continuous-time domain. In view of this point, the peak filter should be tuned for robustness while maintaining the stability of the overall system.

3.4. Repetitive Controller

Repetitive control (RC) is a well-known control method for systems subjected to periodic disturbance and reference. Tomizuka et al. [29] presented a discrete-time repetitive controller that can remedy vibrations at a specific frequency and its resonance frequencies. Because unavoidable rotating vibration is generated during the grinding process, the repetitive controller was designed to suppress the vibration. The configuration of the repetitive controller of this work is shown in Figure 7. The $P(z^{-1})$ is the plant that was identified using the method described in Section 2.3. The $C_R(z^{-1})$ is a signal generator, which can be formulated by the internal model principle, as follows:

$$C_R(z^{-1}) = \frac{z^{-N}}{1 - z^{-N}} \tag{17}$$

where N implies the delay unit of the controller, which is related to the frequency to be suppressed. The $F(z^{-1})$ is the feed forward controller designed with zero-phase error tracking control (ZPETC) [30], which is used to eliminate the dynamics of the plant without changing the phase response. The $Q(z^{-1})$ is a low-pass filter designed used to suppress the amplification of high frequency caused by model mismatching. The filter can be expressed as follows:

$$Q(z^{-1}) = \frac{(1 + z^{-1})^n (1 + z)^n}{4^n} \tag{18}$$

where n is a parameter that can adjust the effect of the filter.

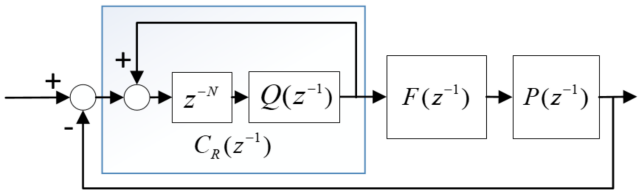

Figure 7. Block diagram of the repetitive controller.

The controller shown in Figure 7 can be reorganized as having $1 - PF$ as the feedback system according to the formulation of the small-gain theory. In this case, the sufficient condition for the overall system to be stable is infinity norm, $1 - PF$, less than one. The added term Q provides the flexibility to tune the performance of the system. Consequently, for the overall system to be stable, the infinity norm of the multiplication of these two terms, $Q(1 - PF)$, should be smaller than one:

$$\|Q(1 - PF)\|_\infty < 1 \tag{19}$$

The criteria implies that the minimal of n is five, which is enough to compensate for the amplification while retaining the ability to suppress the target.

The sensitivity function of the system can be obtained as follows:

$$S(z^{-1}) = \frac{1}{1 + P(z^{-1})F(z^{-1})\frac{Q(z^{-1})^{-N}}{1 - Q(z^{-1})z^{-N}}} \tag{20}$$

Substituting the terms into the equation yields the following:

$$S(z^{-1}) = 1 - Q(z^{-1})z^{-N} \tag{21}$$

The sensitivity function satisfies the internal model principle of the periodic signal; therefore, the function converges to zero and the performance of the controller is theoretically ensured.

Before implementation, there was still a problem that needed to be solved. The repetitive controller can be seen as an integrator because of the feedback loop in the signal generator $C_R(z^{-1})$. With rapid iteration, the system can face a saturation problem that leads to an overshoot and unstable performance. Therefore, an anti-windup structure was added to the system, as shown in Figure 8. The structure is activated only when the command value is beyond the limitations of the system. By subtracting the command value before and after clamping, the result can function as feedback to cease the process of integration and thereby improve the performance of the system.

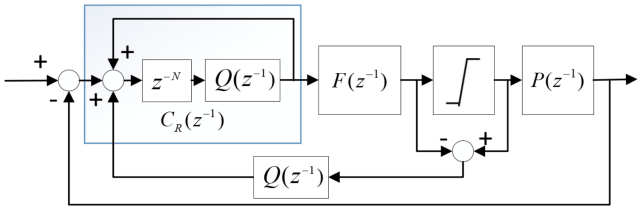

Figure 8. Block diagram of the repetitive controller with anti-windup structure.

Although the repetitive controller is suitable for periodic signals, the working frequency has to be known in advance for construction. Section 3.1 presents that the frequency to be suppressed is related to the grinding-wheel rotating speed. Based on this observation, a connection between the choice of rotating speed and controller design can be established. The parameters should be tuned for rotating speed while maintaining robustness for speed variation during the grinding process.

3.5. Simulation Results

To verify the performance of the controllers described above, the model was simulated, its performance was analyzed, and its dynamic characteristic was explored in Matlab® with Simulink, as shown in Figure 9. Using different force-control methods, the model was set to track a force of 30 N, followed by a reduction to 20 N. Moreover, to make the simulation as realistic as possible, a periodic disturbance which consisted of a base frequency and a resonance frequency was added at the output of the plant to simulate the force vibration caused by the interaction between the grinding wheel and the workpiece.

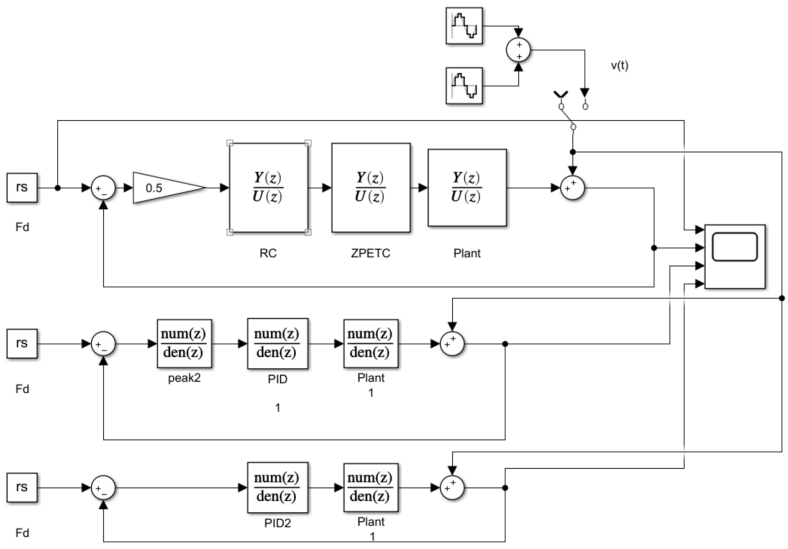

Figure 9. Block diagram of the model built in Matlab® Simulink.

Figure 10 shows the tracking results of the model in six scenarios—the performance of the three control methods with or without disturbance. As illustrated in Figure 8, when there was no disturbance, the controllers all had a fast settling time and a stable tracking performance. However, things changed when the disturbance was added to the simulation. The repetitive controller clearly has the best performance among all. Figure 8 show that PID controller and PID controller with a peak filter has a poor capability to handle the disturbance and could barely eliminate its effect. Although the peak filter can suppress the base frequency, the resonance frequency still variated the tracking performance while the repetitive controller reduced the magnitude of the oscillation caused by the disturbance with different frequency.

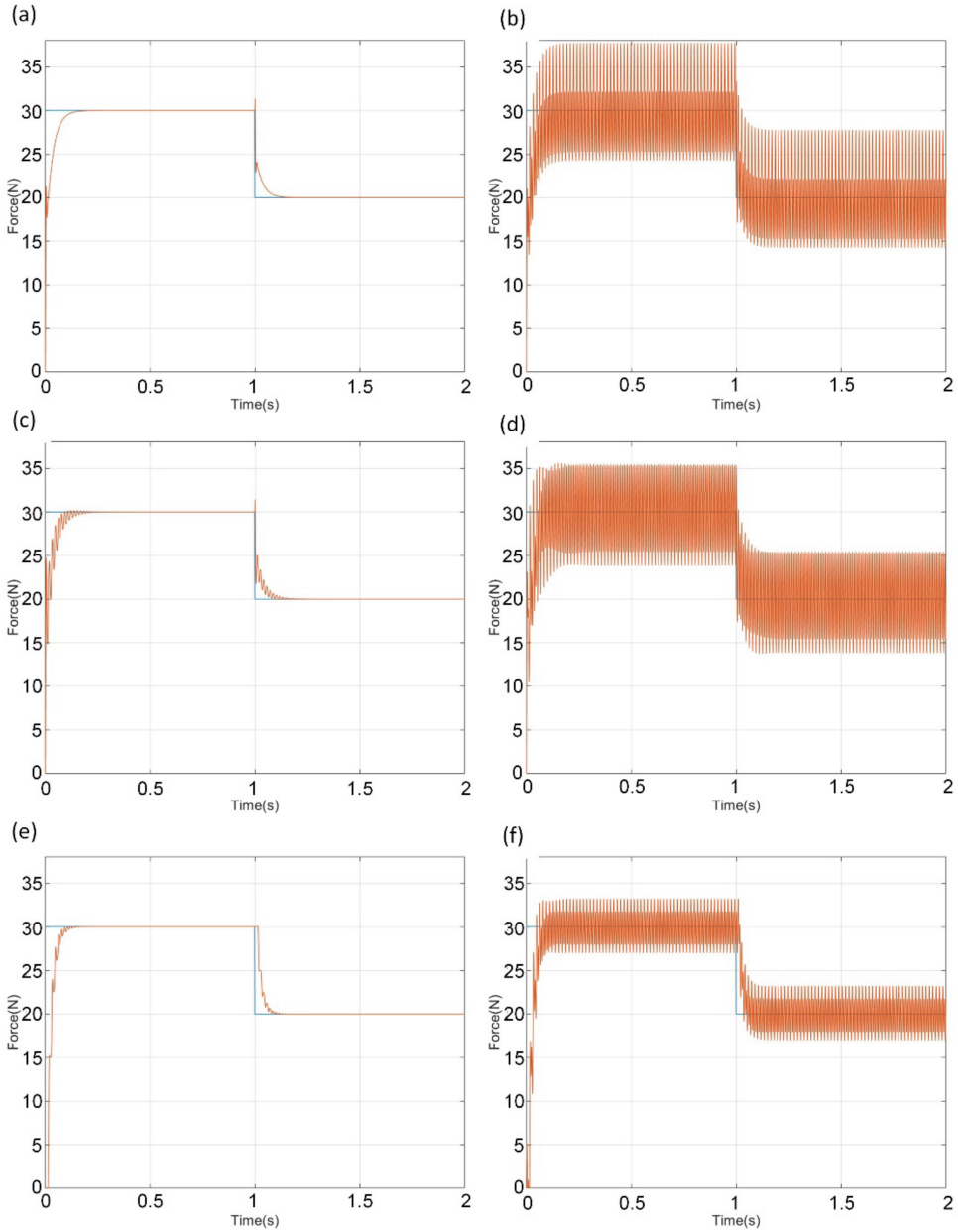

Figure 10. Simulation results of the model: (**a**) PID controller w/o disturbance; (**b**) PID controller with disturbance; (**c**) PID controller and peak filter w/o disturbance; (**d**) PID controller and peak filter with disturbance; (**e**) Repetitive controller w/o disturbance; (**f**) Repetitive controller with disturbance.

4. Experimental Results

4.1. Experimental Setup

The grinding tool was fabricated, and its performance was evaluated experimentally. The six-axis industrial manipulator (TM5-700, Techman Robot Inc., Taipei, Taiwan) shown in Figure 11 was used to mount a workpiece of size 100 mm × 100 mm × 2 mm to be grinded by the grinding tool. A grinding wheel of 180 grit and 100 mm diameter was utilized. A multi-axis force sensor (200 N, Wacoh-Tech Inc., Tokyo, Japan) was also installed on the end of the manipulator to measure the grinding force on the workpieces. The grinding tool was fixed on the table. The manipulator was programmed to move along a straight path with a set feed rate and grinding path. The surface roughness of the workpiece was measured using a surface-roughness tester (SJ-210, Mitutoyo, Kanagawa, Japan).

Figure 11. The grinding experimental setup.

4.2. Parameter Optimization

Before the experiments were conducted, the parameters of the grinding tool had to be decided, which significantly determine the grinding performance. In [31], Hammann et al. proposed an equation for the material removal rate, which consists of several of the most influential parameters that are commonly used in the traditional grinding process. Based on the equation and the limit of the experimental environment, the following four parameters were chosen for optimization: feed rate, rotating speed of the grinding wheel, grinding normal force, and grinding angle. The maximum and the minimum of each parameter were set based on existing research and the limits of the equipment, and the average of the two extreme values was selected as well. As summarized in Table 1, three levels were set for each of the four parameters, so there exist 81 combinations. To simplify the experimental testing process and reduce the testing combinations, the Taguchi method [32] was adopted. Using the L9 orthogonal array, the necessary experiments were reduced to nine combinations instead of 81, as shown in Table 2, which significantly reduced the time and resource cost. Furthermore, the Taguchi method provides a different approach to analyze the experimental data with statistics. Each combination of L9 was experimentally conducted several times, and Table 2 presents the means and standard deviations (STD) of the surface roughness of the grinding experiments.

Table 1. Set levels of the grinding parameters.

Levels	Feed Rate	Rotating Speed (rpm)	Normal Force (N)	Grinding Angle (deg)
1	Command 1	2500	5	20
2	Command 2	3000	10	30
3	Command 3	3900	15	45

Table 2. L9 parameter combinations and grinding experimental results.

Exp.	Feed Rate	Rotating Speed	Normal Force	Grinding Angle	Ra (N)	STD (N)
1	1	1	1	1	3.948	0.255
2	1	2	2	2	3.705	0.647
3	1	3	3	3	4.137	0.914
4	2	1	2	3	4.984	0.252
5	2	2	3	1	6.648	1.165
6	2	3	1	2	4.348	0.550
7	3	1	3	2	7.002	0.492
8	3	2	1	3	6.437	0.664
9	3	3	2	1	6.612	0.635

Table 3 sorts the performance of every parameter and analyzes the influence of changes in levels based on the data presented in Table 2. The table reveals that the feed rate has the greatest influence, followed by the grinding normal force, the grinding angle, and finally, the rotating speed of the grind wheel. The feed rate has over 50% of the overall improvement, which is even more than the sum of the rest parameters. The rotating speed and the grinding angle can barely improve the result. In other words, the feed rate and the normal force are the primary targets to adjust. To sum up, the feed rate should be slow, the rotating speed should be fast, the normal force should be small, and the grinding angle should be 30 degrees. Based on the experimental results, the experiment that utilized the best combination was conducted. The Ra was measured as 2.908 μm, which was indeed better than all the experimental results shown in Table 2. Thus, the parameters in the sense of the Taguchi method were considered optimized. The experiments described in the following section utilized the optimized parameter combination.

Table 3. Analysis of the grinding experimental data.

	Ra (μm)			
	Feed Rate	Rotating Speed of the Grind Wheel	Grinding Normal Force	Grinding Angle
Level 1	3.930	5.312	4.911	5.736
Level 2	5.327	5.597	5.101	5.019
Level 3	6.684	5.033	5.929	5.186
E 1–2	1.397	0.285	0.189	−0.717
E 2–3	1.357	−0.564	0.829	0.167
range	2.754	0.285	1.018	0.550
rank	1	4	2	3
%	59.8	6.2	22.1	11.9

4.3. Experimental Results

4.3.1. Force Tracking under Different Control Methods

In the experiments, the manipulator was programed to grind the workpiece along a straight line in the x-axis direction at a given time, lift and move the workpiece a short distance along the y-axis, and then another straight line was grinded until the surface of the workpiece was completely grinded. Three control methods were evaluated—a PID force controller, a PID force controller with a peak filter, and a repetitive controller. Note that the grinding process has large variations owing to material, surface finish level, speed, etc. It would be difficult to perform quantitative comparisons across different control methods reported by different groups. Thus, as in most of the reported literature, the PID control strategy would be included as the baseline. To guarantee a fair comparison, the real grinding force was measured using the force sensor installed between the workpiece and the manipulator. The desired force was set to 5 N.

Table 4 shows the force-tracking performance of three methods. The PID force controller exhibits an average force of 6.140 N, which implies that the error is 1.14 N. The added peak filter reduces the error to 0.151 N, which also reduces the STD of the force from 3.215 N to 2.457 N, a 23.6% improvement. The repetitive controller has an error of 0.015 N, and the STD of the force is 1.496 N, a 53.5% improvement in comparison with the PID controller.

Table 4. The contact force between the workpiece and the grinding tool using different force control methods.

	Mean (N)	**STD (N)**
PID control	−6.140	3.215
PID control & peak filter	−5.151	2.457
Repetitive control	−5.015	1.496

Figure 12 plots the force spectrums of the three controllers. It can be observed that the magnitude of the targeted 65 Hz was reduced by the peak filter by 11.1% and reduced by the repetitive controller by 71.3%, and the formants were suppressed at the cost of a slight amplification of the non-periodic frequency region. In summary, the PID controller can track the desired force stably but it becomes vulnerable when facing the disturbance. The peak filter can slightly improve performance. The repetitive controller has the best performance due to the signal generator and the compensation of the feedforward structure.

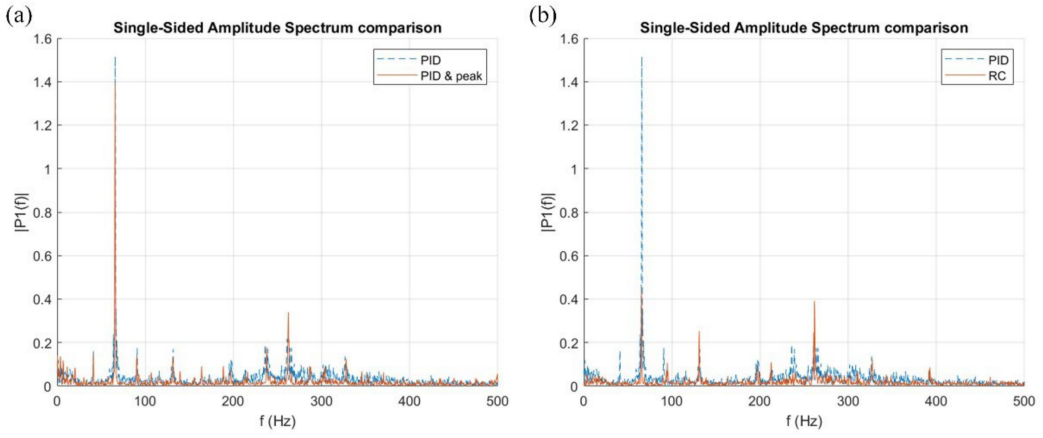

Figure 12. Force amplitude spectrum of the grinding tool using (**a**,**b**) PID force control, (**a**) PID force control with peak filter (PID & peak), and (**b**) repetitive control (RC).

4.3.2. Surface Roughness under Different Control Methods

Other than the force-tracking performance, surface roughness was measured for comparison. Three indicators were calculated to evaluate the surface roughness—Ra, Rz, and Rq. Ra is the arithmetic average of the absolute values of the roughness profile ordinates, and Rz is the arithmetic mean value of the single roughness depths of consecutive sampling lengths. Rq is the root mean square of the surface roughness. For every experiment, the workpiece was divided into nine sections. In each section, the surface roughness was measured using these three indicators. Figure 13 shows the workpieces grinded under three control methods, and Table 5 lists the averaged roughness measures. The photos in Figure 13 were taken under the same condition. Note that Figure 13 is illustrative, and the difference among photos using a visual cue is small and hard to differentiate. Thus, the quantitative analysis is executed using the measurement of surface roughness, as listed in Table 5. Among the three control methods, the PID force controller had the worst performance, while repetitive control had the best performance judging from all three criteria. Compared with the PID controller, the added peak filter improved the surface roughness by about 20%, and the repetitive controller improved that for about 43%. Combined with the force tracking results, the phenomenon that better force tracking performance implies better surface roughness is supported. Therefore, it was confirmed that by suppressing the frequency of the rotating speed, the force disturbance can be reduced, which proves that the main factor of the force disturbance is the grinding plate and its rotating speed.

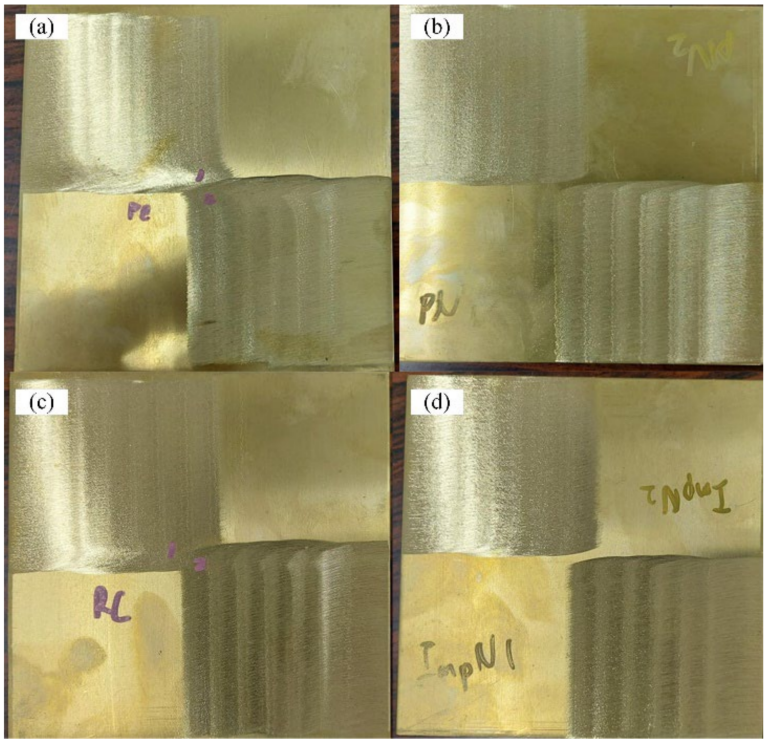

Figure 13. The brass workpiece (**a**) and the grinded workpieces using PID force control (**b**), PID force control with peak filter (**c**), and repetitive control (**d**).

Table 5. Surface roughness of the grinded workpieces using three different force control methods.

	Ra (μm)	Rz (μm)	Rq (μm)
PID control	4.476	26.732	5.609
PID control & peak filter	3.565	21.040	4.519
Repetitive control	2.573	18.630	3.218

4.3.3. Grinding Performance on Curved Surfaces

To further demonstrate the advantage of using the force-controlled grinding tool, a grinding experiment on a commercial polished brass faucet was conducted, as shown in Figure 14. The automatic defect detection of the grinded parts such as the faucet [33] as well as automatic repairing are important works in the field of industrial automation. e Because the faucet has a complex and curvy surface, the grinding path has to follow the normal vector of the surface to avoid collision and maintain the correct contact condition with the surface. Under these circumstances, position error is most likely to occur during the grinding process. Owing to the constraint of geometrical space, a smaller grinding wheel, as shown in Figure 14, was utilized for collision avoidance. The grinding wheel was 300 grit. On the other hand, using different types of grinding wheels can also verify the robustness of the proposed grinding tool.

Figure 14. The grinding process (**a**) and the brass faucet (**b**).

The faucet was grinded using the grinding tool with two control methods, namely a no-force controller (i.e., a fixed relative position between the grinding wheel and the grinding tool body) and the repetitive controller. The grinding path is identical in both cases. Figure 15 shows the grinded surface of the faucets. Currently, we do not have access to a surface-roughness tester that can measure the curvy surface, so the performance of the controller can only be qualitatively judged by the appearance of the faucet. The appearance of the faucet grinded by the grinding tool with the repetitive controller had a uniform surface texture; in contrast, the one grinded by the grinding tool without force control had an irregular texture. Moreover, the coverage of the grinded surface is irregular, and the surface close to the boundary was not processed. Thus, the repetitive force controller has better performance. Note that it is expected that the appearance of the grinded surface is not as good as that of the original polished surface because the latter is a result of a finer surface-treatment process.

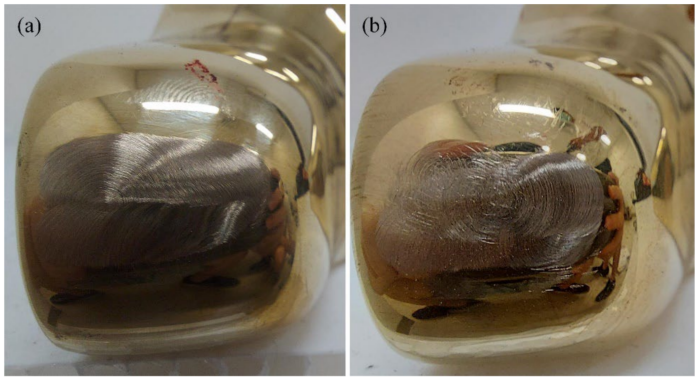

Figure 15. The grinded workpieces using (**a**) the repetitive control and (**b**) no force control.

5. Conclusions and Future Work

In this paper, we designed a grinding tool capable of actively controlling the grinding contact force in real time. The control capability was achieved by adding one controllable linear DOF within the grinding tool. The mechanism of the tool was designed to have the added linear DOF act independently with the original rotary DOF for grinding, thus providing control simplicity. The dynamic model of the grinding tool was constructed, and its parameters were experimentally identified. After understanding the dynamic-force response of the tool, a peak filter and a repetitive controller were designed to suppress the fundamental oscillating frequency, achieving a smooth grinding fabrication process. The proposed grinding tool was fabricated, and its performance was experimentally evaluated. The experimental results show that the force-tracking performance of the repetitive controller averaged a 0.015 N error in the 5 N setting and an STD of 1.496 N. Compared with the PID force controller, the STD of the force showed an improvement of 53.5%, and the force at the target-suppressing frequency was suppressed by 71.3%. In addition, the surface roughness was improved by about 43%, confirming the effectiveness of the proposed grinding tool and control strategy.

Further work can be done to improve the system. The interaction dynamics of the grinding process between the workpiece and the grinding tool can be added to the developed dynamic model. The relation between the model's parameters and the resulting grinding quality, such as surface roughness, can be investigated as well.

Author Contributions: Data curation, Y.-H.L. and M.-W.L.; formal analysis, Y.-H.L.; investigation, M.-W.L.; project administration, P.-C.L.; resources, P.-C.L.; supervision, P.-C.L.; validation, Y.-H.L. and M.-W.L.; writing—original draft, Y.-H.L.; writing—review and editing, P.-C.L. All authors have read and agreed to the published version of the manuscript.

Funding: This work is supported by Ministry of Science and Technology (MoST), Taiwan, under contract: MOST 108-2634-F-002-002-, MOST 109-2634-F-002-039-, and MOST 110-2634-F-002-038-.

Acknowledgments: The authors wish to express their gratitude to Yuan-Chieh Lo and Chih-Hsuan Shih from Industrial Technology Research Institute for useful discussions and HoCheng Cooperation for providing faucet workpieces from the fabrication line.

Conflicts of Interest: The authors declare no conflict of interest.

References

1. Patarinski, S.P.; Botev, R.G. Robot force control: A review. *Mechatronics* **1993**, *3*, 377–398. [CrossRef]
2. Hecker, R.L.; Liang, S.Y. Predictive modeling of surface roughness in grinding. *Int. J. Mach. Tools Manuf.* **2003**, *43*, 755–761. [CrossRef]
3. Chang, H.-C.; Wang, J.-J.J. A stochastic grinding force model considering random grit distribution. *Int. J. Mach. Tools Manuf.* **2008**, *48*, 1335–1344. [CrossRef]
4. Li, H. Experimental study of surface roughness on abrasive belt grinding. In Proceedings of the 2011 International Conference on Electronic & Mechanical Engineering and Information Technology, Harbin, China, 12–14 August 2011; Volume 6, pp. 3010–3013.

5. Rasim, M.; Mattfeld, P.; Klocke, F. Analysis of the grain shape influence on the chip formation in grinding. *J. Mater. Process. Technol.* **2015**, *226*, 60–68. [CrossRef]
6. Qi, J.; Chen, B. Surface Roughness Prediction Based on the Average Cutting Depth of Abrasive Grains in Belt Grinding. In Proceedings of the 2018 3rd International Conference on Mechanical, Control and Computer Engineering (ICMCCE), Huhhot, China, 14–16 September 2018; pp. 169–174.
7. Wang, Y.-H.; Lo, Y.-C.; Lin, P.-C. A Normal Force Estimation Model for a Robotic Belt-grinding System. In Proceedings of the 2020 IEEE/ASME International Conference on Advanced Intelligent Mechatronics (AIM), Boston, MA, USA, 6–10 July 2020; pp. 1922–1928.
8. Zhang, B.C.; Katinas, C.C.; Shin, Y.C. Robust Wheel Wear Monitoring System for Cylindrical Traverse Grinding. *IEEE/ASME Trans. Mechatron.* **2020**, *25*, 2220–2229. [CrossRef]
9. Xu, X.; Chen, W.; Zhu, D.; Yan, S.; Ding, H. Hybrid active/passive force control strategy for grinding marks suppression and profile accuracy enhancement in robotic belt grinding of turbine blade. *Robot. Comput. Manuf.* **2021**, *67*, 102047. [CrossRef]
10. Zhang, H.; Li, L.; Zhao, J.; Zhao, J. The hybrid force/position anti-disturbance control strategy for robot abrasive belt grinding of aviation blade base on fuzzy PID control. *Int. J. Adv. Manuf. Technol.* **2021**, *114*, 3645–3656. [CrossRef]
11. Dai, S.; Zhao, Y.; Ji, W.; Mu, J.; Hu, F. Constant force control for aluminum wheel hub grinding based on ESO + backstepping. *Ind. Robot. Int. J. Robot. Res. Appl.* **2021**. online ahead of print. [CrossRef]
12. Kumar, N.; Rani, M. Neural network-based hybrid force/position control of constrained reconfigurable manipulators. *Neurocomputing* **2021**, *420*, 1–14. [CrossRef]
13. Xu, X.; Zhu, D.; Zhang, H.; Yan, S.; Ding, H. Application of novel force control strategies to enhance robotic abrasive belt grinding quality of aero-engine blades. *Chin. J. Aeronaut.* **2019**, *32*, 2368–2382. [CrossRef]
14. Fazeli, M.; Sadigh, M.J. Adaptive hybrid position/force control for grinding applications. In Proceedings of the 2012 IEEE International Conference on Cyber Technology in Automation, Control, and Intelligent Systems (CYBER), Bangkok, Thailand, 27–31 May 2012; pp. 297–302.
15. Lee, K.; Buss, M. Force Tracking Impedance Control with Variable Target Stiffness. *IFAC Proc. Vol.* **2008**, *41*, 6751–6756. [CrossRef]
16. Jung, S.; Hsia, T.; Bonitz, R. Force Tracking Impedance Control of Robot Manipulators under Unknown Environment. *IEEE Trans. Control Syst. Technol.* **2004**, *12*, 474–483. [CrossRef]
17. Zhang, T.; Yu, Y.; Zou, Y. An Adaptive Sliding-Mode Iterative Constant-force Control Method for Robotic Belt Grinding Based on a One-Dimensional Force Sensor. *Sensors* **2019**, *19*, 1635. [CrossRef] [PubMed]
18. Lu, Z.; Kawamura, S.; Goldenberg, A. Sliding mode impedance control and its application to grinding tasks. In Proceedings of the IROS '91:IEEE/RSJ International Workshop on Intelligent Robots and Systems '91, Osaka, Japan, 3–5 November 1991; Volume 1, pp. 350–355.
19. Kuo, Y.-L.; Huang, S.-Y.; Lan, C.-C. Sensorless Force Control of Automated Grinding/Deburring Using an Adjustable force regulation mechanism. In Proceedings of the 2019 International Conference on Robotics and Automation (ICRA), Montreal, QC, Canada, 20–24 May 2019; pp. 9489–9495.
20. Liao, L.; Xi, F.; Liu, K. Modeling and control of automated polishing/deburring process using a dual-purpose compliant toolhead. *Int. J. Mach. Tools Manuf.* **2008**, *48*, 1454–1463. [CrossRef]
21. Mohammad, A.E.K.; Hong, J.; Wang, D. Design of a force-controlled end-effector with low-inertia effect for robotic polishing using macro-mini robot approach. *Robot. Comput. Manuf.* **2018**, *49*, 54–65. [CrossRef]
22. Xiao, C.; Wang, Q.; Zhou, X.; Xu, Z.; Lao, X.; Chen, Y. Hybrid Force/Position Control Strategy for Electromagnetic based Robotic Polishing Systems. In Proceedings of the Chinese Control Conference CCC, Guangzhou, China, 27–30 July 2019; pp. 7010–7015. [CrossRef]
23. Ma, Z.; See, H.-H.; Hong, G.-S.; Ang, M.H.; Poo, A.-N.; Lin, W.; Tao, P.-Y.; Short, J.S. Control and modeling of an end-effector in a macro-mini manipulator system for industrial applications. In Proceedings of the 2017 IEEE International Conference on Advanced Intelligent Mechatronics (AIM), Munich, Germany, 3–7 July 2017; pp. 676–681.
24. Zhang, X.; Chen, H.; Yang, N.; Lin, H.; He, K. A structure and control design of constant force polishing end actuator based on polishing robot. In Proceedings of the 2017 IEEE International Conference on Information and Automation (ICIA), Macau, China, 18–20 July 2017; pp. 764–768.
25. Lin, Y.H.; Liu, M.W.; Lin, P.C. Development of a grinding tool with contact-force control capability. In Proceedings of the International Conference on Advanced Robotics and Intelligent Systems (ARIS), Taipei City, Taiwan, 18–19 August 2021.
26. Hsu, J.-D.; Tzou, Y.-Y. Modeling and Design of a Voice-Coil Motor for Auto-Focusing Digital Cameras Using an Electromagnetic Simulation Software. In Proceedings of the 2007 IEEE Power Electronics Specialists Conference, Orlando, FL, USA, 17–21 June 2007; pp. 939–944.
27. Rabiner, L.R.; Gold, B.; Yuen, C. *Theory and Application of Digital Signal Processing*; Prentice-Hall: Hoboken, NJ, USA, 2016.
28. Chen, T.; Francis, B.A. *Optimal Sampled-Data Control Systems*; Springer Science and Business Media LLC: Berlin/Heidelberg, Germany, 1995.
29. Tomizuka, M.; Tsao, T.-C.; Chew, K.-K. Analysis and Synthesis of Discrete-Time Repetitive Controllers. *J. Dyn. Syst. Meas. Control* **1989**, *111*, 353–358. [CrossRef]
30. Tomizuka, M. Zero phase error tracking algorithm for digital control. *J. Dyn. Syst. Meas. Control* **1987**, *109*, 65–68. [CrossRef]
31. Hammann, G. *Modellierung des Abtragsverhaltens Elastischer, Robotergeführter Schleifwerkzeuge*; Springer: New York, NY, USA, 1998.

32. Taguchi, G. Quality engineering (Taguchi methods) for the development of electronic circuit technology. *IEEE Trans. Reliab.* **1995**, *44*, 225–229. [CrossRef]
33. Liu, M.-W.; Lin, Y.-H.; Lo, Y.-C.; Shih, C.-H.; Lin, P.-C. Defect Detection of Grinded and Polished Workpieces Using Faster R-CNN. In Proceedings of the 2021 IEEE/ASME International Conference on Advanced Intelligent Mechatronics (AIM), Online, 12–16 July 2021; pp. 1290–1296.